Observations of the Current Sheet Heating in X-ray during a Solar Flare

A.A Reva [ID],[1] S.A. Bogachev [ID],[1] I.P. Loboda [ID],[1] A.S. Ulyanov,[1] and A.S. Kirichenko [ID][1]

[1]*Space Research Institute,*
Profsoyuznaya 84/32,
117997, Moscow, Russia

Submitted to ApJ

ABSTRACT

In the solar corona, magnetic reconnection occurs due to the finite resistivity of the plasma. At the same time, resistivity leads to ohmic heating. Therefore, the reconnecting current sheet should heat the surrounding plasma. This paper presents experimental evidence of such plasma heating caused by magnetic reconnection. We observed the effect during a C1.4 solar flare on 16 February 2003 at the active region NOAA 10278, near the solar limb. Thanks to such a location, we successfully identified all the principal elements of the flare: the flare arcade, the fluxrope, and, most importantly, the presumed position of the current sheet. By analyzing the monochromatic X-ray images of the Sun obtained by the *CORONAS-F*/SPIRIT instrument in the Mg XII 8.42 Å spectral line, we detected a high-temperature ($T > 4$ MK) emission at the predicted location of the current sheet. The high-temperature emission appeared during the CME impulsive acceleration phase. We believe that this additionally confirms that the plasma heating around the current sheet and magnetic reconnection inside the current sheet are strongly connected.

Keywords: Solar corona (1483); Solar x-ray emission (1536); Solar coronal mass ejection (310); Solar flares (1496)

1. INTRODUCTION

Plasma in the solar corona has such a low resistivity that its motion can be treated in the approximation of the ideal magneto-hydrodynamic (MHD). In this approximation, the connectivity of the magnetic field is conserved: two points that belonged to the same field line will continue to belong to the same field line during plasma motion (see chapter 2 in Priest 2014).

Nonetheless, plasma in the solar corona has non-zero resistivity, and, therefore, the connectivity of the magnetic field lines can change. The most important manifestation of this process is magnetic reconnection: a mutual annihilation of two magnetic lines of opposite polarities at the 'magnetic separator.'

Changes of the coronal magnetic field induce the electric current inside the separator. This current prevents reconnection of the magnetic field lines. If the magnetic

field continues to change, the separator will bifurcate into a current sheet: a thin layer of electric current. Eventually, due to the finite resistivity of plasma, the induced current will slowly dissipate, and the magnetic structure will slowly relax to a potential configuration. This process is called 'steady reconnection' (see chapter 1 in Somov 2006).

If the magnetic energy is accumulated faster than it is dissipated by ohmic heating, the current sheet size will increase. Eventually, the current sheet can reach such a size that it becomes unstable, and the whole amount of accumulated energy will be released catastrophically through the 'impulsive reconnection.'

Impulsive reconnection is a central element of the standard model of a solar flare (Carmichael 1964; Sturrock 1966; Hirayama 1974; Kopp & Pneuman 1976). In this model, before the flare begins, the active region has the following configuration: a loop arcade, a fluxrope (cylindrical twisted magnetic structure) above the arcade, and a current sheet between the arcade and the fluxrope (see Figure 1). The flare starts when the cur-
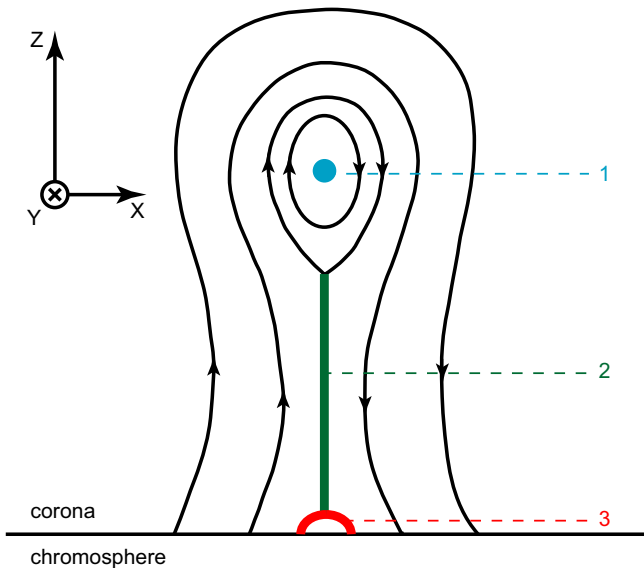
Corresponding author: Anton Reva
reva.antoine@gmail.com

Figure 1. Standard flare/CME model. 1) the fluxrope; 2) the current sheet; 3) the flare arcade.

rent sheet becomes unstable, and impulsive reconnection begins inside it. The reconnection process produces two plasma flows, one of which pushes the fluxrope up and may lead to a coronal mass ejection (CME). At the same time, inside the reconnection region, the electrons are accelerated by the induced electric field. The accelerated electrons move along the magnetic field lines towards the chromosphere, where they slow down, heat plasma, and produce a bremsstrahlung hard X-ray (HXR) emission. The heated plasma fills the magnetic loops above the chromosphere, making them visible in soft X-ray and EUV spectral ranges.

The current sheet is a vital element of the standard flare model. At the same time, it is one of the hardest objects on the Sun to observe. One of the main reasons is that there are no effective ways to directly measure magnetic fields or electric currents in the solar corona. Another reason is that the current sheet is a very thin structure. It has a huge size in the Y and Z directions in Figure 1, but negligible size along the X axis (several meters, or even several cm). So the plasma emission inside the current sheet is expected to be negligible compared to the emission of the surrounding coronal plasma.

Despite this, several authors reported signatures of the current sheet observed during solar flares. In the imaging observations, a long thin linear structure above the flaring active region is usually interpreted as a current sheet signature (Lin et al. 2005; Savage et al. 2010; Reeves & Golub 2011; Zhu et al. 2016; Seaton et al. 2017). Besides that, an elongated double Y-shaped dark structure can appear below the CME core

in the Fe 171 Å images (Reva et al. 2016a). In the spectroscopic observations, researchers consider a high-temperature emission from the presumed location of the current sheet—below the CME core and above the flaring active region—as a signature of the current sheet (Ciaravella et al. 2002; Ko et al. 2003; Ciaravella & Raymond 2008). Recently, Warren et al. (2018) presented multi-wavelength observations of the current sheet using both imaging (AIA; Lemen et al. 2012) and spectroscopic (EIS; Culhane et al. 2007) instruments.

In all the examples listed above, the authors reported, not the direct observations of the current sheet, but rather its indirect observational signatures. Among such indirect evidence, one of the most important is the plasma heating in the vicinity of the current sheet caused by the ohmic heating due to the finite resistivity of the coronal plasma.

Mechanisms of such heating are actively studied with the theoretical models and the numerical MHD simulations. These studies showed that ohmic heating (Reeves et al. 2010, 2019), adiabatic compression (Birn et al. 2009; Reeves et al. 2019), and turbulence (Ye et al. 2020) can effectively heat plasma inside the current sheet. Some of the thermal energy accumulated inside the current sheet may leak away due to thermal conduction, which will heat the surrounding plasma and widen the visible size of the current sheet ('thermal halo'; Yokoyama & Shibata 1998; Seaton & Forbes 2009; Reeves et al. 2010). Using MHD simulations, Reeves et al. (2010) showed that thermal conduction could leak up to 50 % of the energy released during the reconnection.

For many reasons, it is hard to experimentally study the relationship between the current sheet heating and magnetic reconnection rate. First of all, as mentioned above, the observations of current sheets (even indirect) are rare. Secondly, most solar telescopes—such as AIA/*SDO* or XRT/*Hinode* (Golub et al. 2007)—cannot detect high-temperature plasma in a monochromatic mode. The hot plasma emission in their images is mixed with a low-temperature background, which complicates the analysis of the heating.

In this work, we report reliable signatures of the plasma heating up to temperatures higher than 4 MK detected in the vicinity of the coronal current sheet in a monochromatic mode. We also experimentally confirmed the relationship between the plasma heating and the reconnection rate, which we derived from the observation of CME acceleration. In section 2, we describe the experimental data used in the research. In section 3, we present the obtained results; then, in section 4, we discuss them and make the conclusions.
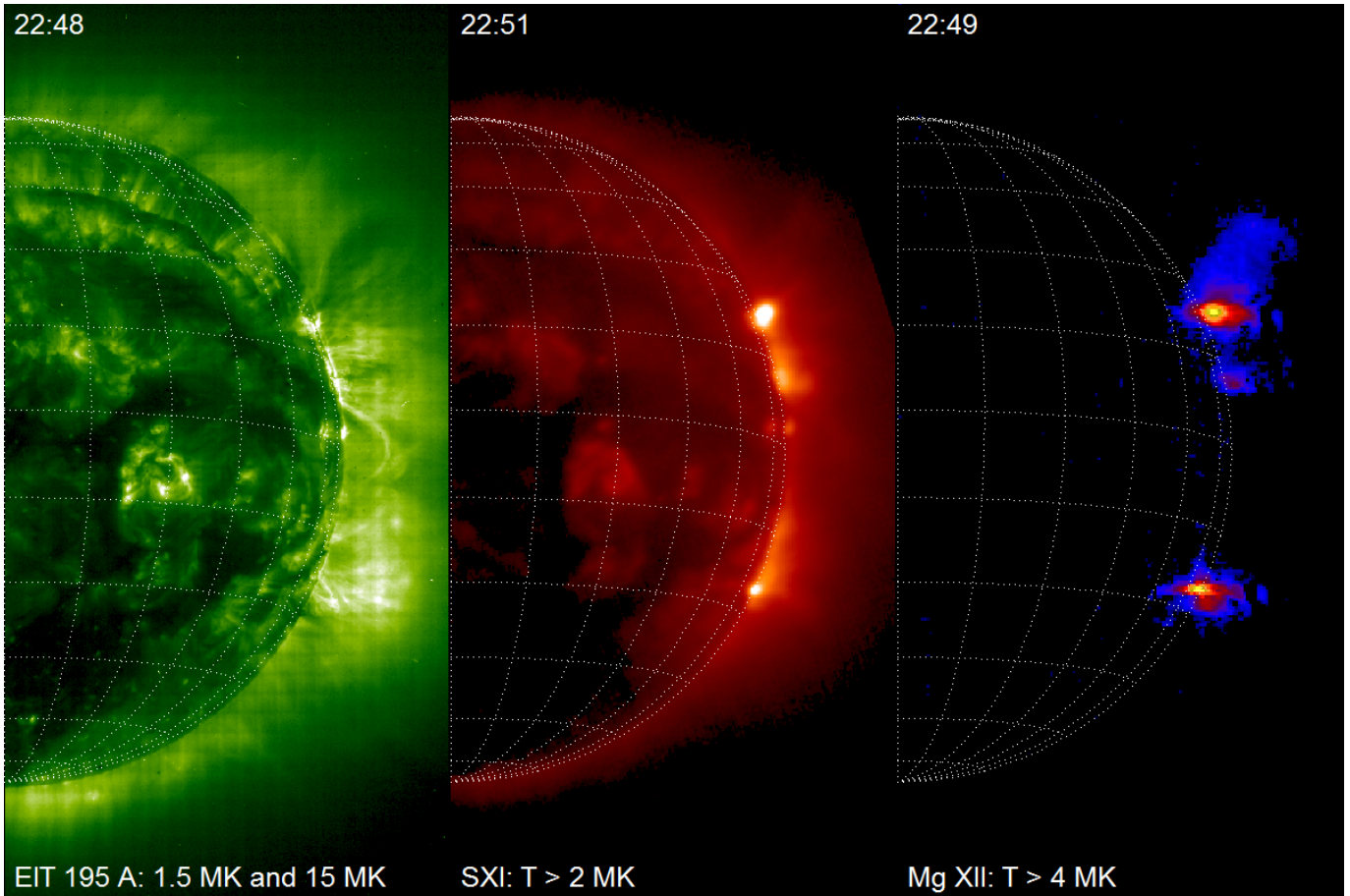
Figure 2. Comparison of the images obtained by the EIT 195 Å (left), SXI (middle), and the Mg XII spectroheliograph (right). The images were taken on 16 February 2003.

2. EXPERIMENTAL DATA

The event (flare and CME) that we have studied in this paper occurred on 16 February 2003 near the western edge of the Sun. To study it, we used several instruments to get most of the information about plasma heating, details of the reconnection process, and CME structure. The full list of data used in the study is presented in Table 1.

The most important instrument for our study was the Mg XII spectroheliograph that operated on board the *CORONAS-F*/SPIRIT satellite from 2001 till 2003 (Oraevsky & Sobelman 2002; Zhitnik et al. 2002). Considering that the instrument may not be well known to some readers, we will briefly describe some of its important features.

The instrument is an imaging spectroheliograph based on Bragg-crystal optics. It obtained monochromatic X-ray images of the solar corona in the Mg XII 8.42 Å spectral line. During the selected period of observations, the spectroheliograph worked with a 2 min cadence and a binned resolution of 8″.

The main feature that distinguishes the Mg XII spectroheliograph from other imaging instruments is its temperature selectivity. The Mg XII 8.42 Å line produces a noticeable signal only at temperatures higher than 4 MK. So, the corresponding images clearly outline the high-temperature plasma on the Sun without any contribution from the low-temperature background (see Figure 2). This gives an effective way to study the plasma heating processes in many objects: large-scale flares (Grechnev et al. 2006; Urnov et al. 2007; Reva et al. 2015), CMEs (Kirichenko & Bogachev 2013; Reva et al. 2017), and even microflares (Reva et al. 2012; Kirichenko & Bogachev 2017a,b; Reva et al. 2018).

It is important to note that the instrument is equipped with a crystal mirror and, therefore, had dispersion. In the Mg XII images, each point of the Sun looks like a short profile of the Mg XII 8.42 Å spectral line. To lessen this effect, we numerically deconvolved the Mg XII images. For more details, see Appendix A.

The pointing system of the *CORONAS-F* spacecraft had a significant residual jitter. To correct it, we used data from the Solar X-ray Imager (SXI; Hill et al. 2005;
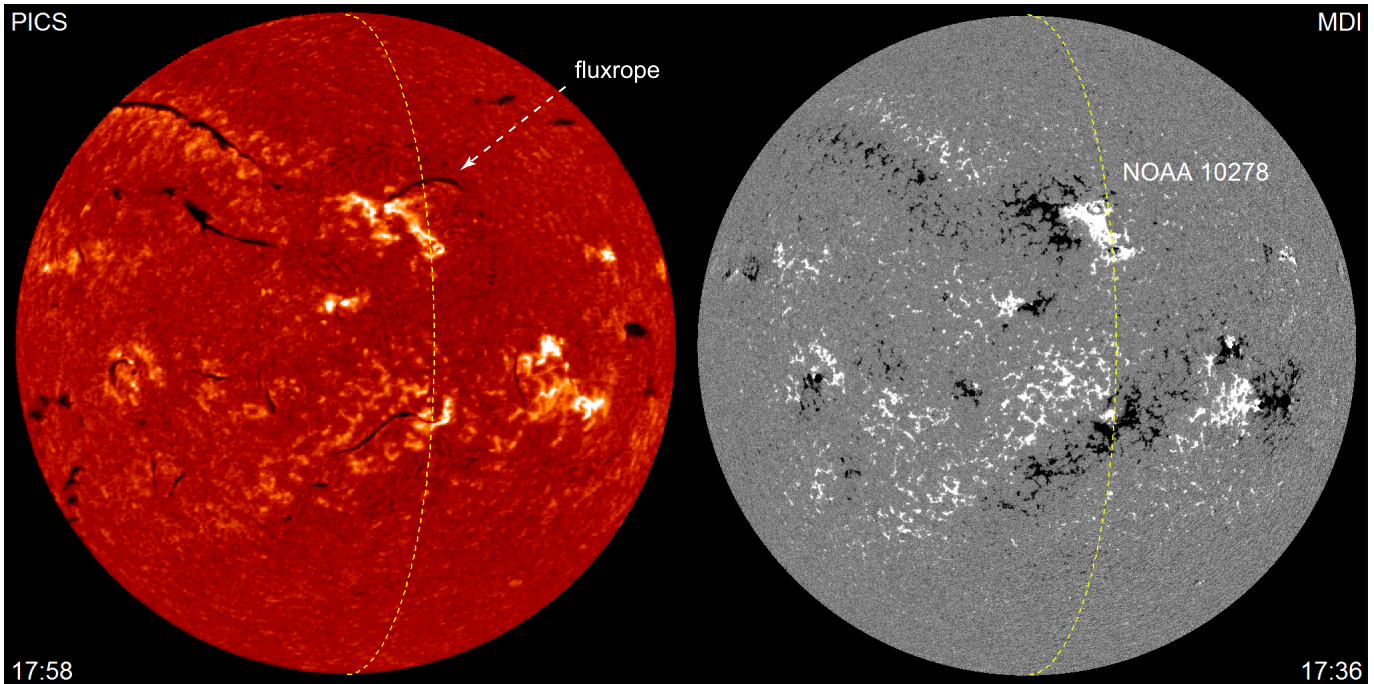
Figure 3. Active region NOAA 10278 on the disc. Left: Hα image obtained with the PICS telescope. Right: magnetogram obtained with MDI. Images were taken on February 11, 2003. The yellow dashed line indicates the position of the limb at 23:00 UT on February 16, 2003.

Table 1. List of instruments.

	Instrument	Reference
Location and dynamics of high-temperature plasma	Mg XII spectroheliograph	Zhitnik et al. (2003)
	SXI	Hill et al. (2005); Pizzo et al. (2005)
Location of the HXR sources	RHESSI	Lin et al. (2002)
CME structure and dynamics	EIT	Delaboudinière et al. (1995)
	TRACE	Handy et al. (1999)
	Mk4	Elmore et al. (2003)
	LASCO	Brueckner et al. (1995)
Magnetic field configuration	MDI	Scherrer et al. (1995)
Prominences and filaments in Hα	PICS	DOI: 10.5065/D65719TR

Pizzo et al. 2005) that worked on board the *GOES-12* satellite. The telescope provided full-disk soft X-ray solar images in the 6-60 Å wavelength range with a spatial resolution of ≈ 10″ and a 5″ pixel size. The 'Be-thin' channel of SXI is sensitive to the same temperatures as the Mg XII spectroheliograph, but with a noticeable contribution of low-temperature background. The orientation of the Sun in the SXI images is known. Using cross-correlation, we determined the shift between the Mg XII images and the 'Be-thin' SXI images. Then we shifted the Mg XII images by the corresponding value to correct the jitter.

During the selected period of observations, all of the SPIRIT telemetry was allocated to the Mg XII data.

This improved the cadence of the observations, but, as a result, the data of other instruments of the SPIRIT complex were not available.

Below we briefly describe other instruments used in this research.

The *Reuven Ramaty High Energy Solar Spectroscopic Imager* (RHESSI; Lin et al. 2002) observes HXR spectra from 3 keV to 17 MeV. Using Fourier-based methods, RHESSI can synthesize HXR images in the same spectral range.

The Extreme ultraviolet Imaging Telescope (EIT; Delaboudinière et al. 1995) on the *Solar and Heliospheric Observatory* (*SoHO*; Domingo et al. 1995) takes solar images at the wavelengths centered at 171, 195, 285,
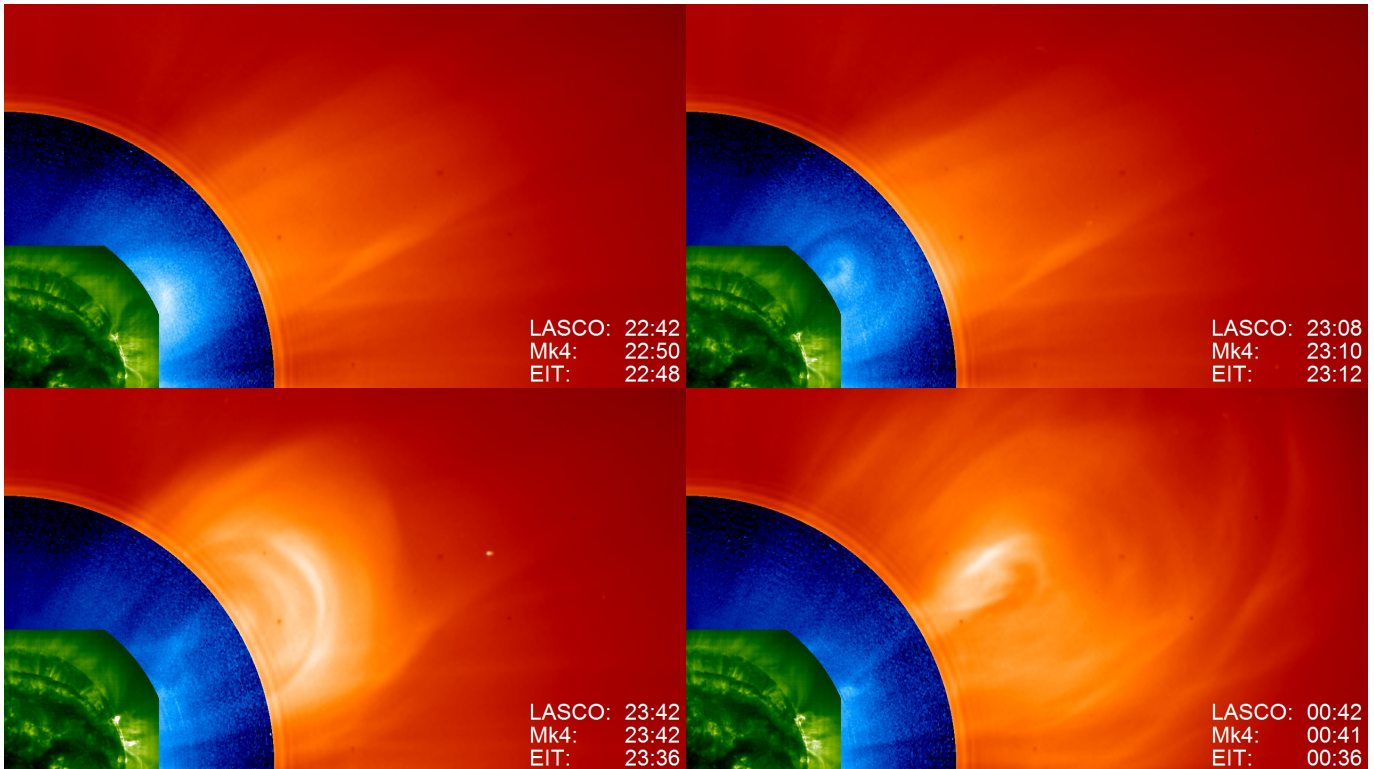
Figure 4. Evolution of the CME. Green: EIT telescope; blue: Mk4 coronagraph; red: LASCO C2 coronagraph.

and 304 Å. The instrument has a pixel size of $2.6''$ and a spatial resolution of $5''$. The EIT had two observational modes: synoptic and 'CME watch.' In a synoptic mode, it takes images in all four channels every 6 hours. In the 'CME watch' mode, the telescope takes images in the 195 Å channel every 12 min.

The Transition Region And Coronal Explorer (TRACE; Handy et al. 1999) is a space-based telescope that observes the Sun in EUV and white-light. It had a limited field of view ($8.5' \times 8.5'$) but a high spatial resolution ($1''$).

Mk4 coronameter is a ground-based instrument located at Mauna Loa Solar Observatory (DOI: 10.5065/D66972C9; Elmore et al. 2003). It builds images of the solar corona from 1.14 to 2.86 $R_\odot$ in the white light (700–900 nm) with a spatial resolution of $5.95''$ and a cadence of 3 min.

Large Angle Spectroscopic Coronagraph (LASCO; Brueckner et al. 1995) is a set of white-light coronagraphs that observe solar corona from 1.1 $R_\odot$ up to 30 $R_\odot$ (C1, 1.1–3 $R_\odot$; C2, 2–6 $R_\odot$; C3, 4–30 $R_\odot$). In 1998, LASCO C1 stopped working, and for this research, only C2 and C3 data are available. Coronagraph C2 has a resolution of $11''$, and C3 has a resolution of $56''$.

The Michelson Doppler Imager (MDI; Scherrer et al. 1995) on the *SOHO* satellite maps the line of sight component of the photospheric magnetic field with a $4''$ resolution and 90-min cadence.

Polarimeter for Inner Coronal Studies (PICS, DOI: 10.5065/D65719TR) is a ground-based instrument located at Mauna Loa Solar Observatory. It takes Hα images (6563 Å) with a field of view of 2.3 $R_\odot$, a spatial resolution of $2.9''$, and a cadence of 3 minutes.

3. RESULTS

3.1. *Flare Topology and Dynamics*

The studied event was a typical solar flare associated with a CME, which developed in full agreement with the standard views on how a solar flare should evolve. This is very important for our study because it is thanks to the standard configuration of the flare we are sure about where the current sheet was located.

Taking this into account, let us describe the flare topology and dynamics. The pre-flare configuration (5 days before the flare) is shown in Figure 3, where the left panel is the Hα image, and the right panel is the corresponding MDI magnetogram. The flare occurred in the active region NOAA 10278. On 11 February 2003, this active region was approximately in the center of the solar disk. The most prominent feature of the active region seen in Hα images (left panel) was a filament that was slightly tilted to the East-West direction and was
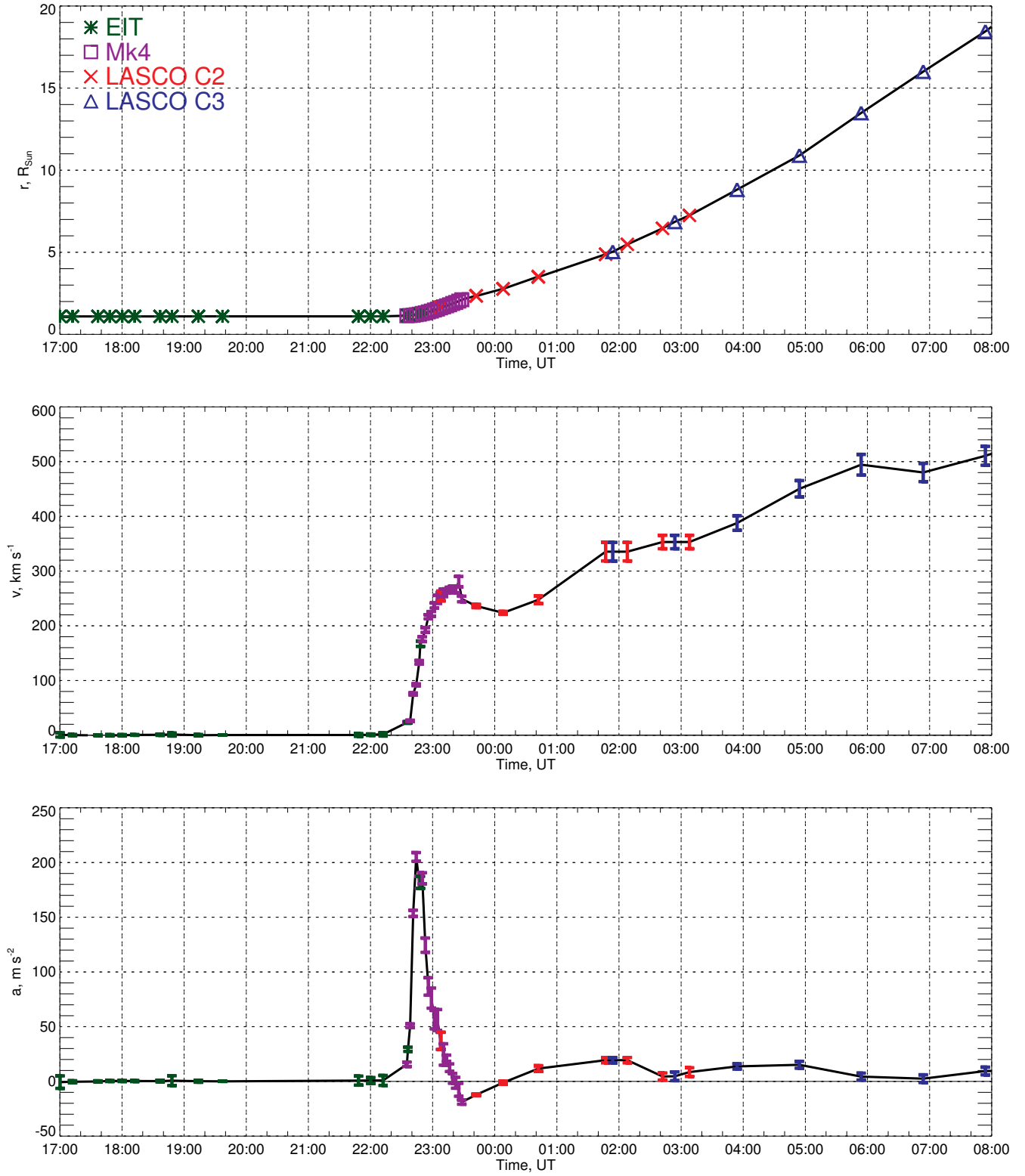
Figure 5. Kinematics of the CME core. Top: the distance between the CME core and Sun's center; middle: the CME core's velocity; bottom: the CME core's acceleration. Green: data of the EIT telescope; purple: data of the Mk4 coronagraph; red: data of the LASCO/C2 coronagraph; blue: data of the LASCO/C3 coronagraph.
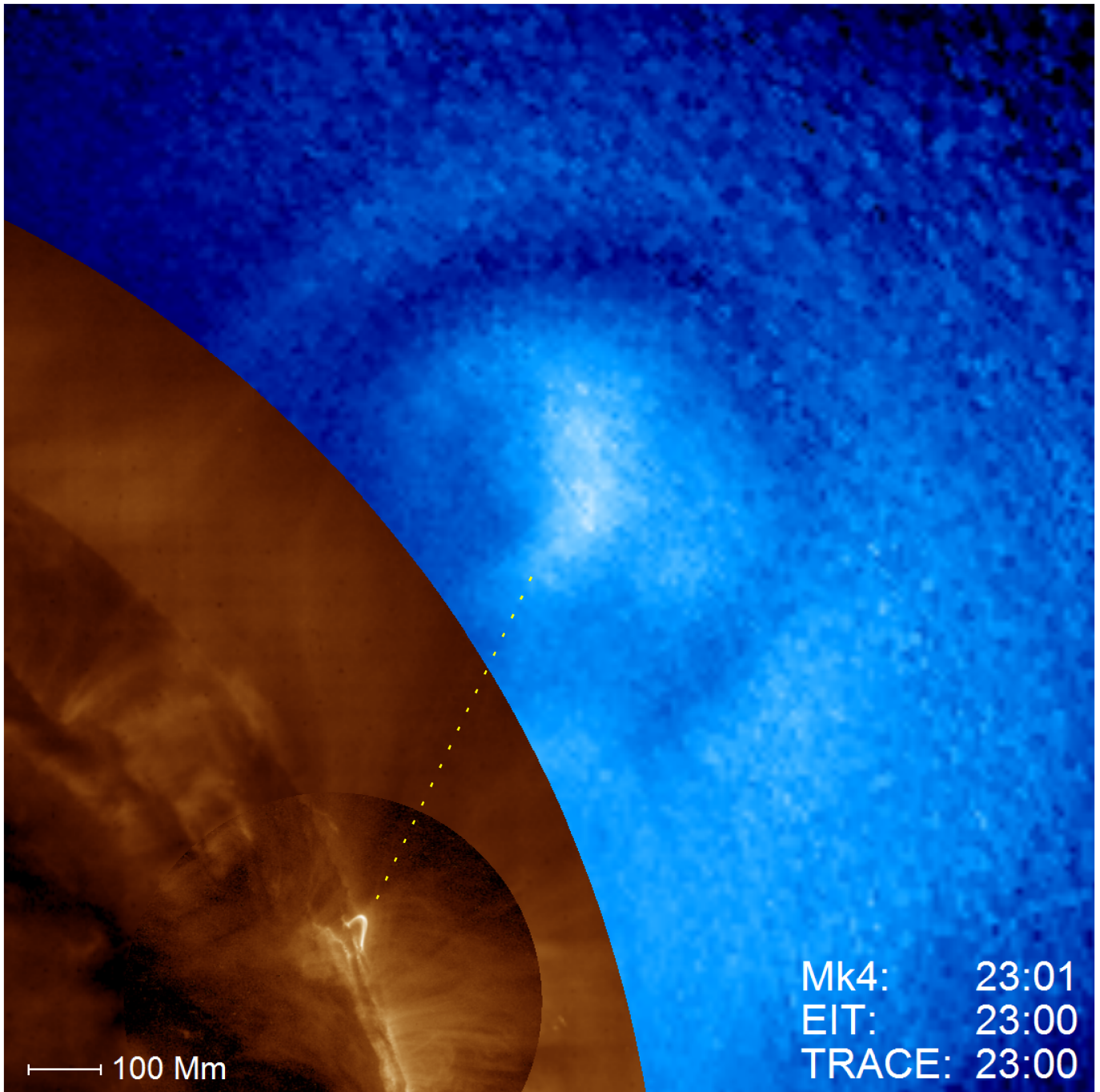
Figure 6. CME topology. Copper inner circle: TRACE image; copper outer circle: EIT image; blue: Mk4 image. The dotted line marks the presumed location of the current sheet. The images were taken on 16 February 2003.

located between two areas of opposite polarities. We match this filament to the fluxrope of the further CME.

This filament was seen in Hα images all five days from February 11 until February 16, when the active region reached the solar limb. At this moment, the region took the same position as in our sketch for the standard flare/CME model (see Figure 1). So, this was the best projection to observe the current sheet.

Approximately at this time, the CME started to erupt. To study this process, we used synthetic images combined from EIT data obtained in EUV and two white light images: one from the Mk4 coronameter and the second one from the LASCO C2 coronagraph (see Figure 4). The CME had a classic 3-part structure in white-light images: bright core, dark cavity, and bright frontal loop (Illing & Hundhausen 1985; Webb & Hundhausen

1987). As we said above, we identify the CME core with the filament (fluxrope) that was seen in the Hα images before the CME (Illing & Athay 1986). In this case, the fluxrope should be aligned along the Y axis in Figure 1.

Observation of the CME motion gives an indirect way to measure the reconnection rate during a solar flare. Generally, we can expect a simple relationship: the faster is the reconnection rate, the faster is the CME acceleration.

Taking this into account, we measured the CME coordinates during its motion (for details of the measurement method, see Appendix B). The result—the CME height, velocity, and acceleration as a function of time—is shown in Figure 5. From these plots, we see that CME evolution consists of three main phases:

1. before ≈ 22:35, the CME structure was stable;

2. from ≈ 22:35 to ≈ 23:10, the CME impulsively accelerated from 0 to 250 km s^{-1}; the acceleration peaked at ≈ 200 m s^{-2};

3. after ≈ 23:10, the CME gradually accelerated to ≈ 500 km s^{-1} during 9 hours with an acceleration of ≈ 10–20 m s^{-2}.

The observed flare topology is consistent with the standard flare model. We can clearly see a flare arcade, a fluxrope, and a cavity that surrounds the fluxrope (see Figure 6). The CME evolution is also consistent with the standard model. It has a stable phase, an impulsive acceleration phase (probably caused by the impulsive reconnection), and a steady acceleration phase (probably caused by the solar wind; Yashiro et al. 2004). Since the studied flare looks and behaves exactly as the standard model predicts, it is natural to assume that a current sheet should exist between the flare arcade and the CME core.

3.2. *Observation of the Plasma Heating*

As we said above, the main goal of this paper was to find clear evidence of plasma heating in the vicinity of the reconnecting current sheet. For this purpose, we carefully checked all the Mg XII images obtained during the studied event. Thanks to the specific temperature sensitivity of the Mg XII spectroheliograph (starting from $T \geq 4$ MK), we consider the corresponding images as a good marker of plasma heating. As soon as the signal appears in a Mg XII image, we can conclude that the plasma temperature increases to 4 MK or higher.

The observed dynamics of hot plasma is shown in Figure 7. We found two high-temperature regions during the flare. The first one (the brightest one) appeared at

21:53 UT and existed for ≈ 5 hours. The region was compact, and its location approximately coincides with the top of the flare loop seen in the TRACE 195 Å image. Plasma heating near the looptop region is a typical feature of a solar flare, and for this reason, we do not consider it in detail. The looptop plasma heating takes place under the current sheet in the so-called 'cusp' region of the magnetic configuration. Such a source is often associated with a looptop hard X-ray emission: another typical detail of a solar flare. The HXR emission appears at the same place (see Figure 7) and at the same time (see Figure 8) as region-1.

The most interesting for us was the second high-temperature region. At 22:28 UT, a faint linear structure appeared above the flare arcade. It gradually increased its length but decreased its intensity. Eventually, the linear structure faded away, reaching the maximal length of 250 Mm. In other parts of the CME, there was no hot plasma.

The hot linear structure was located between the flare arcade and the CME core (observed in the Mk4 images) and inside the dark cavity observed in the EIT images (see Figure 9). Such a location coincides with the presumed position of the current sheet that should exist during CME.

Two important features distinguish this second plasma region from the first one. The first feature is the location. Region-2 is clearly not associated with the top of the flare loop and with a 'cusp' region. Another feature is a significant difference in brightness and size. Region-2 is much larger than the compact region-1, but, despite this, it is much fainter. The peak flux of the linear structure was ≈ 4 % of the peak flux from the compact, bright source (see Figure 8), while the brightness ratio (pixel intensity ratio) was ≈ 0.5–1 %. This seriously justifies that region-1 and region-2 were heated by two different mechanisms. We want to emphasize that region-2 is observed simultaneously with region-1. So, we cannot explain them as two consecutive stages of the same heating mechanism.

The timing of the plasma heating is in good agreement with the CME motion. The flare begins at ≈ 21:53 UT when the plasma heating starts near the looptop region of the arcade, and the HXR emission starts to rise (see Figure 8). We did not find any signatures of plasma heating in the current sheet (region-2) during this stage. Approximately 30 minutes later, the second stage associated with the CME motion started. At ≈ 22:30 UT, the CME impulsively accelerated from zero up to $v \approx 300$ km s^{-1} with an acceleration of $a \approx 100$–200 m s^{-2}. Due to the fast CME motion, the current sheet should be elongating rapidly in the Z-direction
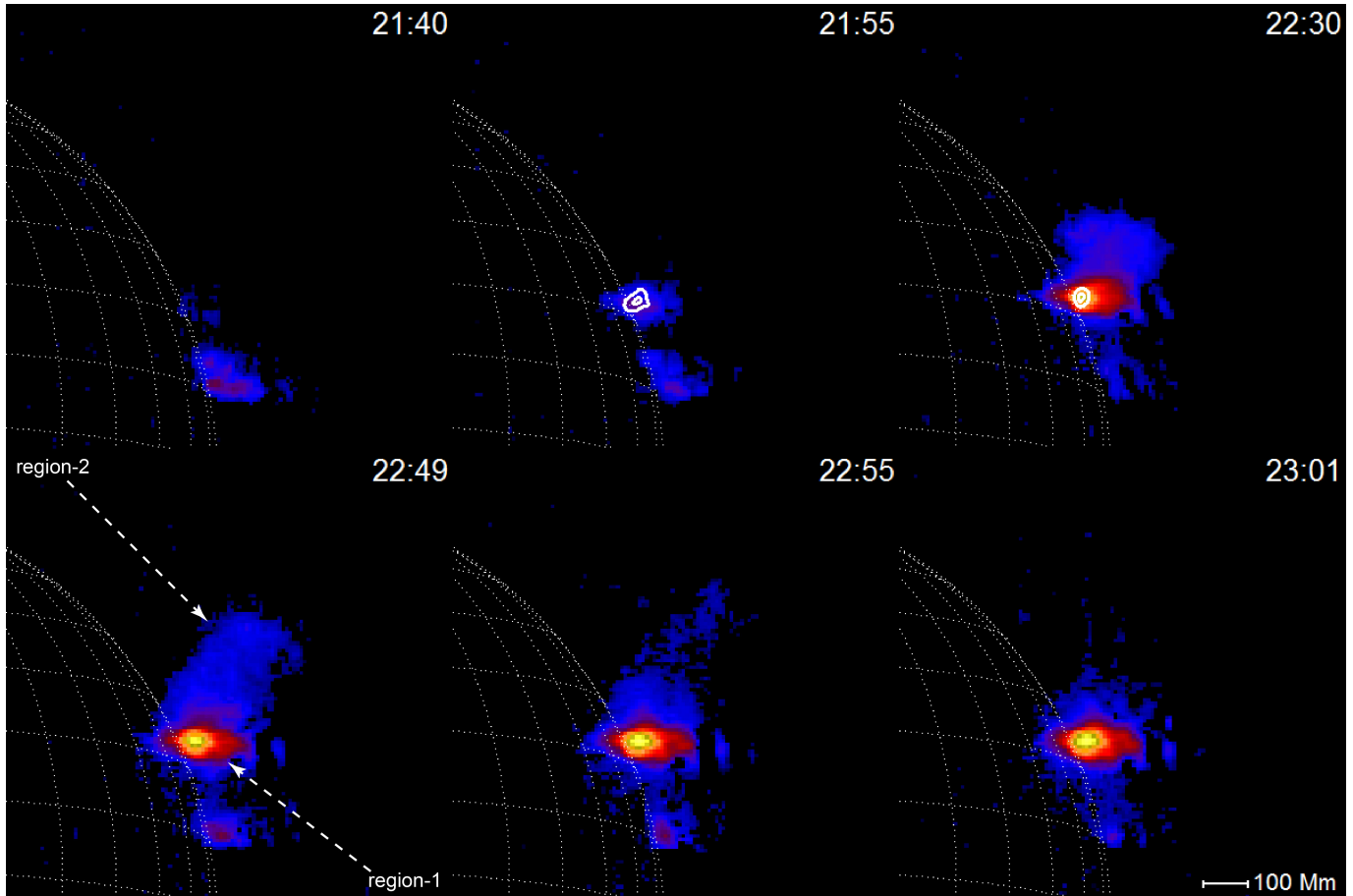
Figure 7. Hot plasma dynamics observed with the Mg XII spectroheliograph. Blue corresponds to low intensities, red and yellow correspond to high intensities. Contours mark the location of the RHESSI 6–12 keV emission.

(see Figure 1), and just at this time, we observed an additional plasma heating around the presumable location of the current sheet. The CME acceleration lasted about 30 minutes, which is in excellent agreement with the observed duration of plasma heating in region-2 (see Figure 10).

Sadly, the RHESSI data were not available during the CME impulsive acceleration (see Figure 8). For this reason, we do not have information about the dynamics of the HXR emission.

4. DISCUSSION AND CONCLUSION

The appearance of high-temperature plasma in the solar corona is typical for solar flares and usually relates to the magnetic reconnection process. Bright sources of thermal X-ray emission usually appear above the top of magnetic loops during the impulsive phase of solar flares. They may be heated by energized electrons or by super-sonic plasma flows.

In a typical magnetic configuration of a flare region, the bright loop-top source is not the only high-temperature region that may appear above the loop dur-

ing a flare. A much fainter but much larger source may appear higher in the corona due to a diffusion of thermal energy from the region of magnetic reconnection.

Usually, this second source (named region-2 in our study) cannot be observed due to its low brightness, which does not allow it to be distinguished from the low-temperature background. We succeeded in this study due to two main factors. The first one is the region's location and orientation: the CME occurred at the solar limb, and the current sheet was aligned along the line of sight. Such a location and orientation are favorable to detect faint emission of the current sheet. The second one is the temperature sensitivity of the Mg XII spectroheliograph. The instrument detects a high-temperature emission without the contribution of low-temperature background.

The low brightness ratio of faint and bright components (~ 1 %) also contributes to the difficulties of the registration. We think that this ratio is typical for flares, but, of course, we have no confirmation of this since only one such event was detected.
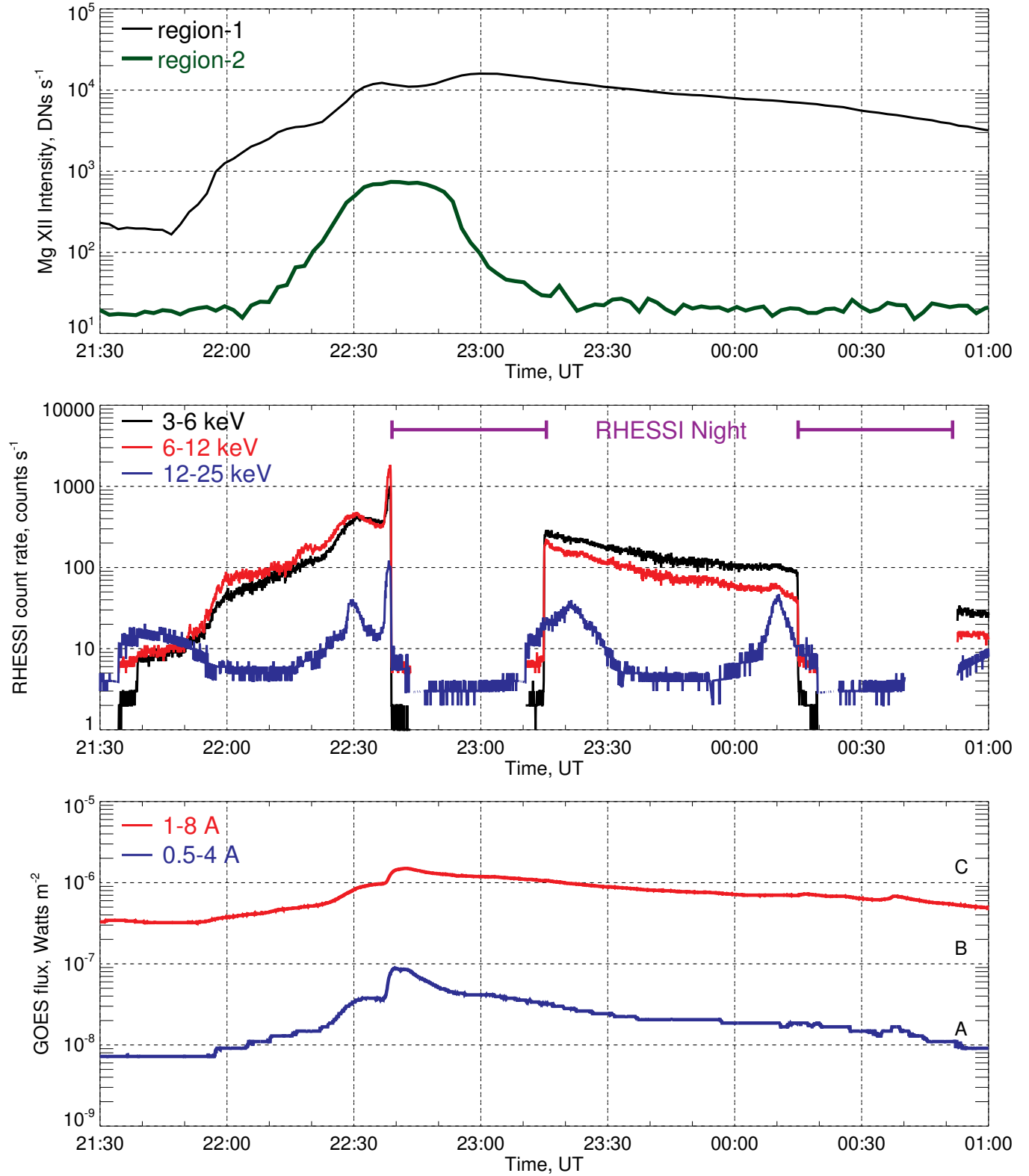
Figure 8. X-ray flux dynamics. Top: the Mg XII lightcurves of region-1 (thin black line) and region-2 (thick black line). Middle: the RHESSI count rates. Black line: 3–6 keV channel; red line: 6–12 keV channel; blue line: 12–25 keV channel. Purple lines mark the RHESSI nights. Bottom: GOES flux. Red line: 1–8 Å channel; blue line: 0.5–4 Å channel.
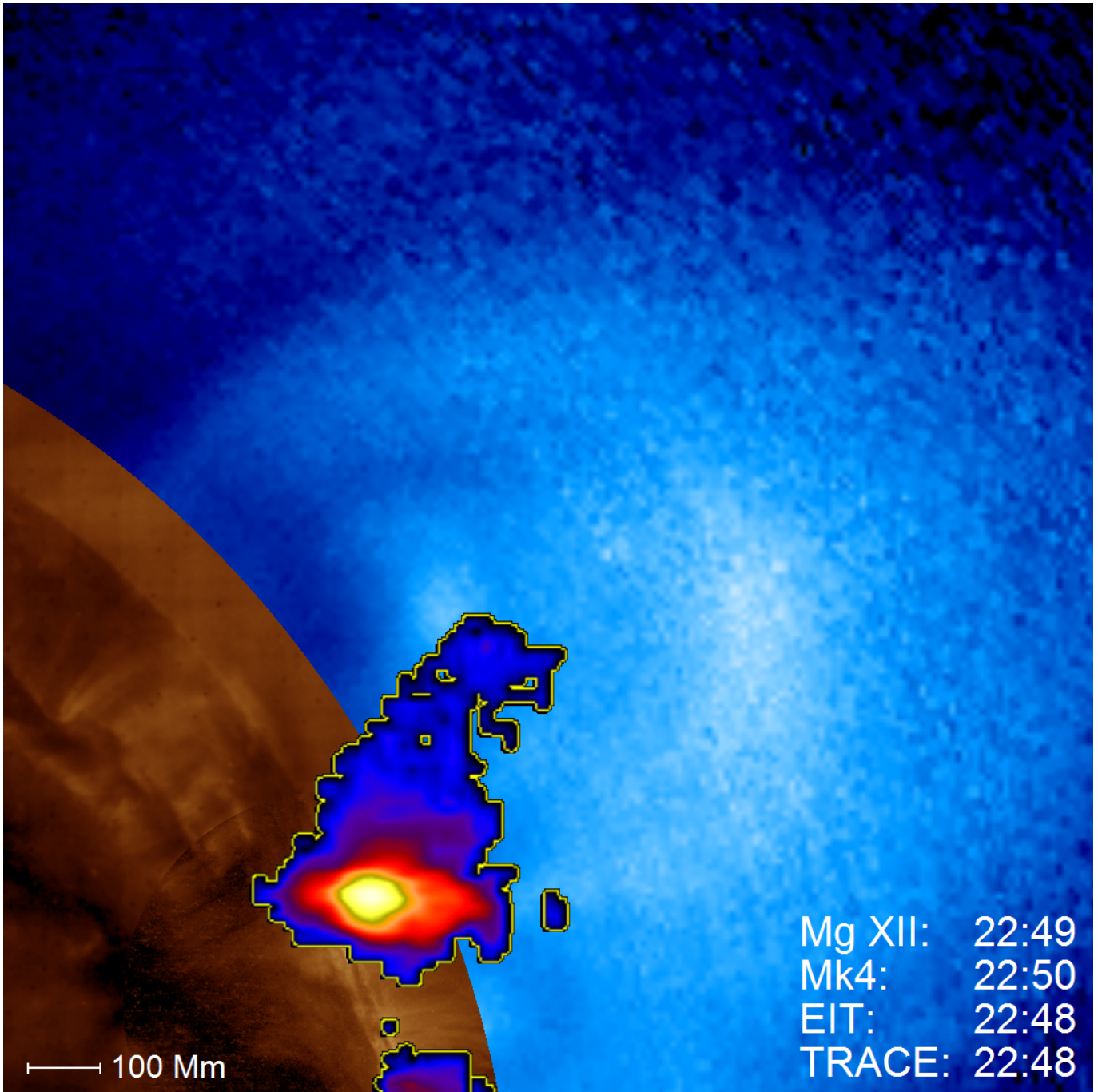
Figure 9. Comparison of the Mg XII, TRACE, EIT, and Mk4 images. Inside yellow contour: signal of the Mg XII spectroheliograph (blue corresponds to low intensities, red and yellow correspond to high intensities). Copper inner circle: TRACE image; copper outer circle: EIT image; blue: Mk4 image. The images were taken on 16 February 2003.

The appearance of the faint component we associate with the heating caused by the reconnection inside the current sheet. Comparison of the emission and CME dynamics confirms this idea. The faint high-temperature component appears approximately at the same time as the CME impulsively accelerates. According to the standard CME model, the CME impulsively accelerates during impulsive reconnection inside the current sheet.

We think that this clearly indicates that the energy for plasma heating in region-2 comes from magnetic reconnection, which is in good agreement with standard views on solar flares.

Another indirect evidence of the connection between heating and reconnection is the relative timing of region-1 and region-2 emissions. Region-2 appears during the rising phase of the Mg XII and GOES fluxes of region-1
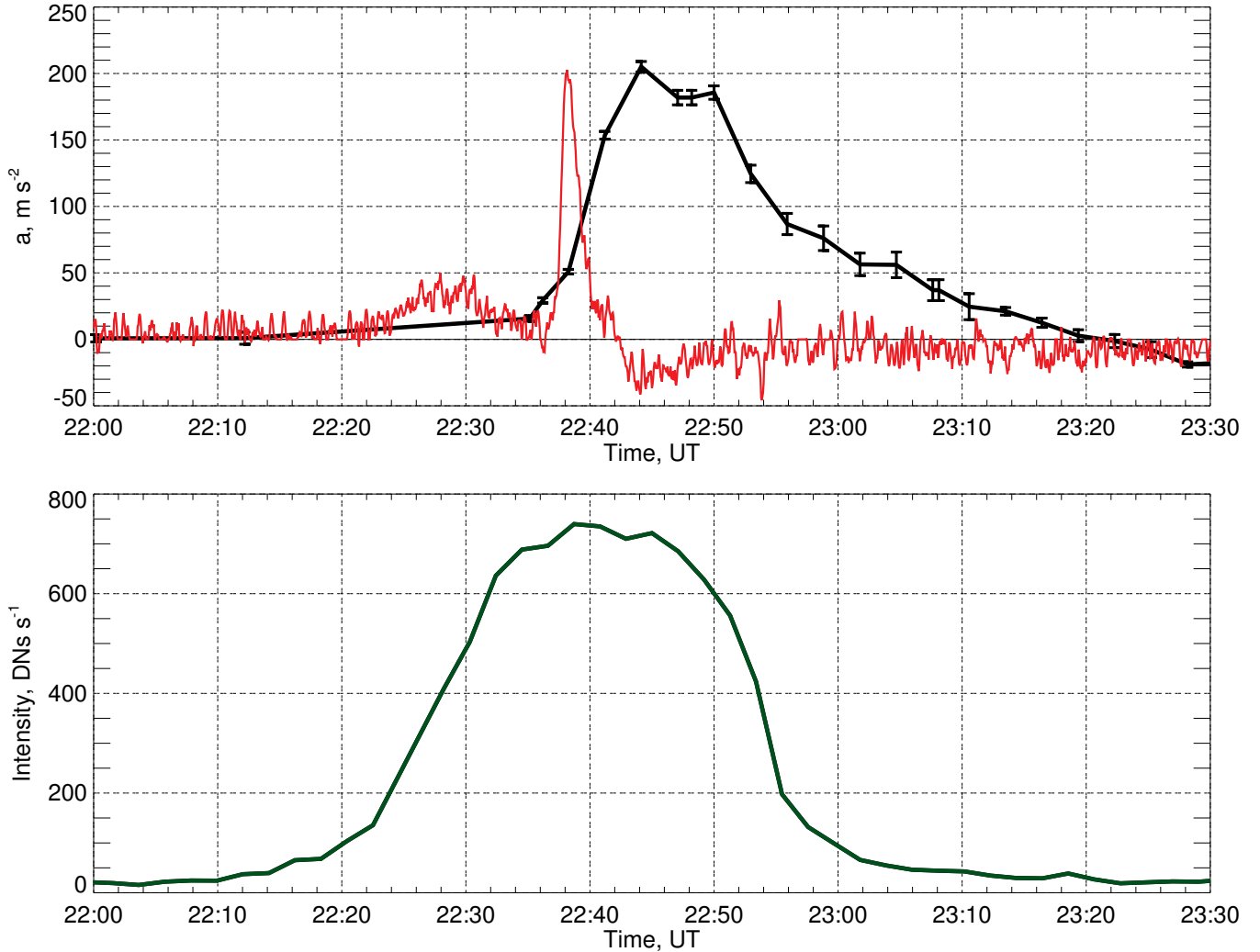
Figure 10. Relative timings of the CME's acceleration (black line at the top), the derivative of the GOES 1–8 Å flux (red line at the top), and the linear structure (region-2) intensity in the Mg XII images (green line at the bottom).

(see Figure 8). According to the Neupert effect (Neupert 1968), the HXR emission of a flare correlates with the derivative of the SXR emission. The GOES 1–8 Å flux derivative—our estimate of the HXR emission—peaks when we observe region-2 (see Figure 10). Since HXR emission is a signature of the reconnection, we think that such a correlation further strengthens our interpretation.

The hot plasma was detected in the previous observations of the current sheets. Ciaravella et al. (2002); Ko et al. (2003); Ciaravella & Raymond (2008) studied current sheets observed with Ultraviolet Coronagraph Spectrometer (UVCS; Kohl et al. 1995) and reported temperatures around 6 MK. The current sheets analyzed by Zhu et al. (2016) and Seaton et al. (2017) had temperatures around 8–10 MK, while the ones analyzed by Hannah & Kontar (2013) and Warren et al. (2018) had temperatures around 10–20 MK. Finally, Landi et al.

(2012) presented observations, in which current sheet temperature never exceeded 3 MK. Most likely, the difference in the current sheet temperatures is caused by the difference in the reconnection rate.

Our conclusion that the current sheet heating is caused by the reconnection inside it is consistent with the MHD theory and simulations (Yokoyama & Shibata 1998; Seaton & Forbes 2009; Reeves et al. 2010). However, it is difficult to compare this conclusion with other experimental works. Current sheet observations are rare, and only a couple of them allow studying the dynamics of the current sheet heating relative to the dynamics of the reconnection.

The first such example is a current sheet observed during an X8.3 flare on 2017 September 10 (Warren et al. 2018). At the time of writing, this is the most detailed observation of the current sheet (see references in Chen et al. 2020). In this event, some re-

connection signatures—the CME impulsive acceleration (Gopalswamy et al. 2018; Veronig et al. 2018), the hard X-ray emission, the derivative of the soft X-ray emission, and the microwave emission (Gary et al. 2018)—correlated with each other and occurred during a small period of time ($\approx$ 15:50–16:00 UT). On the other hand, other reconnection signatures—downflows (Longcope et al. 2018) and turbulence (Cheng et al. 2018; Warren et al. 2018) inside the current sheet—were observed for $\approx$ 1 hour after the first reconnection signatures appeared ($\approx$ 16:00–17:00 UT). The current sheet itself appeared after the first reconnection signatures ($\approx$ 16:00 UT) and hot plasma inside it was observed for $\approx$ 1 hour in the 94 Å channel of Solar Ultraviolet Imager (SUVI; Seaton & Darnel 2018).

Another example is the current sheet observed during the CME on 2009 April 17 (Reva et al. 2016a). The event was observed with the TESIS EUV telescope that build images of the solar corona in the Fe 171 Å line up to distances of 2 $R_\odot$ from the Sun center (Kuzin et al. 2011; Reva et al. 2014). The current sheet looked like a double Y-shaped darkening in the Fe 171 Å images. Such darkening indicates that the current sheet is heated (although, it is not clear up to what temperature). The heating (darkening) occurred simultaneously with the CME impulsive acceleration (signature of the reconnection). At the start of the CME impulsive acceleration phase, GOES and SphinX (Gburek et al. 2011) registered a short duration flux increase.

All of these three examples—this work, Reva et al. (2016a), and Warren et al. (2018)—exhibit a similar pattern. During the CME eruption, a short-duration reconnection signatures appear, which are followed by the long-duration reconnection signatures. The heating inside the current sheet starts approximately when the short-duration reconnection signature appears. The hot plasma inside the current sheet is observed during the lifetime of the long-duration reconnection signatures. These similarities support our conclusion that heating inside the current sheet is caused by the reconnection.

However, there are differences between these events. In this work and Reva et al. (2016a), the heating starts slightly before the short-duration reconnection signatures; in Warren et al. (2018), it starts after. In this work and Reva et al. (2016a), the impulsive CME acceleration is a long-duration signature; in Warren et al. (2018), it is a short-duration signature. These differences and the fact that some reconnection signatures have short duration and some long duration show that the reconnection dynamics has a complex structure, which may vary from one event to another.

We are sure that the energy for the current sheet heating comes from the magnetic reconnection. However, the exact mechanism of the heating is unclear. As we said in the Introduction, ohmic heating (Reeves et al. 2010, 2019), adiabatic compression (Birn et al. 2009; Reeves et al. 2019), and turbulence (Ye et al. 2020) can heat current sheet. Sadly, our data don't allow us to determine the heating mechanism.

Another issue that we would like to discuss is the relative weakness of the studied flare. Usually, current sheets are observed during strong flares (X and M classes), while the flare in this work is only C1.4. Figure 3 shows that most of the flaring active region was visible. Even if we take into account partial occultation by the disk, the flare would still be of a C class.

We believe that the studied event is an example of reconnection heating occurring as a universal process in flares from C to X class. Most likely, reconnection heating is less intense in weak flares than in strong ones, and, therefore, plasma is heated to lower temperatures and has lower emission measure. As a result, such heating is rarely observed in weak flares because it is difficult to detect faint hot emission.

We think that monochromatic imagers similar to the Mg XII spectroheliograph—for example, see Kuznetsov et al. (2016); Kirichenko et al. (2021); Reva et al. (2021)—can help us study reconnection heating. We hope that such instruments will be created in future and that they will improve our understanding of the processes occurring inside the current sheets during solar flares.
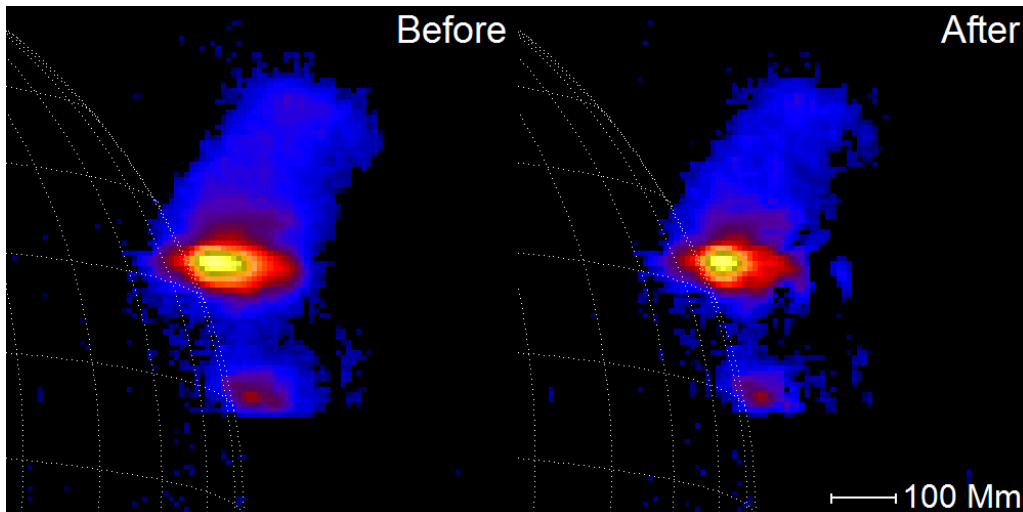
Figure 11. Deconvolution of the Mg XII images. Left: image before deconvolution; right: image after deconvolution.

APPENDIX

A. MG XII DECONVOLUTION

The Mg XII spectroheliograph used Bragg crystal optics. As a result, the instrument has dispersion: its images are a convolution of the spatial component with the profile of the Mg XII 8.42 Å line. More details about this effect could be read in Kuzin et al. (1994) or Reva et al. (2021).

The Mg XII $\lambda = 8.42$ Å line is a Ly-α doublet of a hydrogen-like Mg ion: $\lambda_1 = 8.4192$ Å ($1s\ ^2S_{1/2} - 2p\ ^2P_{3/2}$) and $\lambda_2 = 8.4246$ Å ($1s\ ^2S_{1/2} - 2p\ ^2P_{1/2}$). The ratio of the line intensity should be 2:1.

The Mg XII images consist of two slightly shifted images overlayed one onto another (see Figure 11a). The majority of the pixels in the Mg XII images do not have a signal: they consist of several isolated hot objects. In the direction of the dispersion, the boundaries of those objects contain only a signal from one of the doublet components. The profile of the doublet components overlaps only inside those objects.

To deconvolve the Mg XII images, we use the following algorithm.

1. We start at the boundary of the image that corresponds to the short wavelengths.

2. For each pixel, we calculate the intensity of the weaker component (divided by two).

3. We subtract this value from the pixel that corresponds to the location of the weaker component of the doublet.

4. We move in the direction of the dispersion to the next pixel that corresponds to a longer wavelength.

5. We repeat steps 2–4 until we reach the boundary of the image.

The result is shown in Figure 11b. The algorithm successfully eliminates the second component of the doublet. The images become less elongated and easier to interpret.

There are several issues that this algorithm does not address. Firstly, it does not deconvolve the line width. It cannot be deconvolved in a straightforward way because the line width is determined by the Doppler broadening, which varies from pixel to pixel. Secondly, the line ratio of the Lyα doublet could deviate from the theoretical value (Sylwester et al. 1986; Laming 1990). If this effect is present, it can distort the deconvolved images. Finally, if significant plasma motions along the line of sight are present, the Doppler shifts will distort the images.

B. CME KINEMATICS MEASUREMENTS

For the measurements of the CME coordinates, we used the data of the EIT telescope, Mk4 coronameter,

and LASCO coronagraphs. We used a simple point-and-click method. To estimate the errors of the measurements, we repeated the procedure nine times for each image.

In the Mk4 and LASCO images, we aimed at the CME core's center. Since the core was not seen in the EIT images, we aimed for the lowest part of the dark cavity in the EIT images.

The coordinates measured in the EIT images (lowest part of the dark cavity) and the white-light images (CME's core) are different parts of the CME. We cannot simply combine these coordinates and compute derivatives (velocity and acceleration). Furthermore, the point-and-click method is subjective, and different instruments image corona differently. The center of the core in images obtained by different instruments corresponds to slightly different parts of the CME. In order

to compute derivatives, we need to recalculate coordinates measured in the EIT images to the CME's core coordinates and adjust the core coordinates measured by different white-light instruments.

To solve the problem, we adopted the method from Reva et al. (2016b). We assumed that the CME expands proportionally and that the temporal dependence of the heights of different parts of the CME could be linearly scaled. Then we picked scaling coefficients so that temporal dependence of the CME core height seamlessly transitions from one instrument to another.

After scaling the data, we numerically differentiated the radial distance and obtained radial velocity. Then we numerically differentiated velocity and obtained acceleration. For the differentiation, we used the local least-square approximation method (Wood 1982; Reva et al. 2017). The result of the measurements is presented in Figure 5.

REFERENCES

Birn, J., Fletcher, L., Hesse, M., & Neukirch, T. 2009, ApJ, 695, 1151, doi: 10.1088/0004-637X/695/2/1151

Brueckner, G. E., Howard, R. A., Koomen, M. J., et al. 1995, SoPh, 162, 357, doi: 10.1007/BF00733434

Carmichael, H. 1964, NASA Special Publication, 50, 451

Chen, B., Yu, S., Reeves, K. K., & Gary, D. E. 2020, ApJL, 895, L50, doi: 10.3847/2041-8213/ab901a

Cheng, X., Li, Y., Wan, L. F., et al. 2018, ApJ, 866, 64, doi: 10.3847/1538-4357/aadd16

Ciaravella, A., & Raymond, J. C. 2008, ApJ, 686, 1372, doi: 10.1086/590655

Ciaravella, A., Raymond, J. C., Li, J., et al. 2002, ApJ, 575, 1116, doi: 10.1086/341473

Culhane, J. L., Harra, L. K., James, A. M., et al. 2007, SoPh, 243, 19, doi: 10.1007/s01007-007-0293-1

Delaboudinière, J., Artzner, G. E., Brunaud, J., et al. 1995, SoPh, 162, 291, doi: 10.1007/BF00733432

Domingo, V., Fleck, B., & Poland, A. I. 1995, SoPh, 162, 1, doi: 10.1007/BF00733425

Elmore, D. F., Burkepile, J. T., Darnell, J. A., Lecinski, A. R., & Stanger, A. L. 2003, in Society of Photo-Optical Instrumentation Engineers (SPIE) Conference Series, Vol. 4843, Polarimetry in Astronomy, ed. S. Fineschi, 66–75, doi: 10.1117/12.459279

Gary, D. E., Chen, B., Dennis, B. R., et al. 2018, ApJ, 863, 83, doi: 10.3847/1538-4357/aad0ef

Gburek, S., Sylwester, J., Kowalinski, M., et al. 2011, Solar Sys. Res., 45, 189, doi: 10.1134/S0038094611020067

Golub, L., Deluca, E., Austin, G., et al. 2007, SoPh, 243, 63, doi: 10.1007/s11207-007-0182-1

Gopalswamy, N., Yashiro, S., Mäkelä, P., et al. 2018, ApJL, 863, L39, doi: 10.3847/2041-8213/aad86c

Grechnev, V. V., Kuzin, S. V., Urnov, A. M., et al. 2006, Solar System Research, 40, 286, doi: 10.1134/S0038094606040046

Handy, B. N., Acton, L. W., Kankelborg, C. C., et al. 1999, SoPh, 187, 229, doi: 10.1023/A:1005166902804

Hannah, I. G., & Kontar, E. P. 2013, A&A, 553, A10, doi: 10.1051/0004-6361/201219727

Hill, S. M., Pizzo, V. J., Balch, C. C., et al. 2005, SoPh, 226, 255, doi: 10.1007/s11207-005-7416-x

Hirayama, T. 1974, SoPh, 34, 323, doi: 10.1007/BF00153671

Illing, R. M. E., & Athay, G. 1986, SoPh, 105, 173, doi: 10.1007/BF00156385

Illing, R. M. E., & Hundhausen, A. J. 1985, J. Geophys. Res., 90, 275, doi: 10.1029/JA090iA01p00275

Kirichenko, A., Kuzin, S., Shestov, S., et al. 2021, Frontiers in Astronomy and Space Sciences, 8, 66, doi: 10.3389/fspas.2021.646895

Kirichenko, A. S., & Bogachev, S. A. 2013, Astronomy Letters, 39, 797, doi: 10.1134/S1063773713110042

—. 2017a, ApJ, 840, 45, doi: 10.3847/1538-4357/aa6c2b

—. 2017b, SoPh, 292, 120, doi: 10.1007/s11207-017-1146-8

Ko, Y.-K., Raymond, J. C., Lin, J., et al. 2003, ApJ, 594, 1068, doi: 10.1086/376982

Kohl, J. L., Esser, R., Gardner, L. D., et al. 1995, SoPh, 162, 313, doi: 10.1007/BF00733433

Kopp, R. A., & Pneuman, G. W. 1976, SoPh, 50, 85, doi: 10.1007/BF00206193

Kuzin, S. V., Andreev, E. A., Korneev, V. V., et al. 1994, in Society of Photo-Optical Instrumentation Engineers (SPIE) Conference Series, Vol. 2283, X-Ray and Ultraviolet Spectroscopy and Polarimetry, ed. S. Fineschi, 242–250, doi: 10.1117/12.193192

Kuzin, S. V., Zhitnik, I. A., Shestov, S. V., et al. 2011, Solar System Research, 45, 162, doi: 10.1134/S0038094611020110

Kuznetsov, V. D., Zelenyi, L. M., Zimovets, I. V., et al. 2016, Geomagnetism and Aeronomy, 56, 781, doi: 10.1134/S0016793216070124

Laming, J. M. 1990, ApJ, 357, 275, doi: 10.1086/168914

Landi, E., Raymond, J. C., Miralles, M. P., & Hara, H. 2012, ApJ, 751, 21, doi: 10.1088/0004-637X/751/1/21

Lemen, J. R., Title, A. M., Akin, D. J., et al. 2012, SoPh, 275, 17, doi: 10.1007/s11207-011-9776-8

Lin, J., Ko, Y.-K., Sui, L., et al. 2005, ApJ, 622, 1251, doi: 10.1086/428110

Lin, R. P., Dennis, B. R., Hurford, G. J., et al. 2002, SoPh, 210, 3, doi: 10.1023/A:1022428818870

Longcope, D., Unverferth, J., Klein, C., McCarthy, M., & Priest, E. 2018, ApJ, 868, 148, doi: 10.3847/1538-4357/aaeac4

Neupert, W. M. 1968, ApJL, 153, L59, doi: 10.1086/180220

Oraevsky, V. N., & Sobelman, I. I. 2002, Astron. Lett., 28, 401, doi: 10.1134/1.1484141

Pizzo, V. J., Hill, S. M., Balch, C. C., et al. 2005, SoPh, 226, 283, doi: 10.1007/s11207-005-7417-9

Priest, E. 2014, Magnetohydrodynamics of the Sun, doi: 10.1017/CBO9781139020732

Reeves, K. K., & Golub, L. 2011, ApJL, 727, L52, doi: 10.1088/2041-8205/727/2/L52

Reeves, K. K., Linker, J. A., Mikić, Z., & Forbes, T. G. 2010, ApJ, 721, 1547, doi: 10.1088/0004-637X/721/2/1547

Reeves, K. K., Török, T., Mikić, Z., Linker, J., & Murphy, N. A. 2019, ApJ, 887, 103, doi: 10.3847/1538-4357/ab4ce8

Reva, A., Shestov, S., Bogachev, S., & Kuzin, S. 2012, SoPh, 276, 97, doi: 10.1007/s11207-011-9883-6

Reva, A., Shestov, S., Zimovets, I., Bogachev, S., & Kuzin, S. 2015, SoPh, 290, 2909, doi: 10.1007/s11207-015-0769-x

Reva, A., Ulyanov, A., Kirichenko, A., Bogachev, S., & Kuzin, S. 2018, SoPh, 293, 140, doi: 10.1007/s11207-018-1363-9

Reva, A. A., Kirichenko, A. S., Ulyanov, A. S., & Kuzin, S. V. 2017, ApJ, 851, 108, doi: 10.3847/1538-4357/aa9986

Reva, A. A., Kuzin, S. V., Kirichenko, A. S., et al. 2021, Frontiers in Astronomy and Space Sciences, 8, 40, doi: 10.3389/fspas.2021.645062

Reva, A. A., Ulyanov, A. S., Bogachev, S. A., & Kuzin, S. V. 2014, ApJ, 793, 140, doi: 10.1088/0004-637X/793/2/140

Reva, A. A., Ulyanov, A. S., & Kuzin, S. V. 2016a, ApJ, 832, 16, doi: 10.3847/0004-637X/832/1/16

Reva, A. A., Ulyanov, A. S., Shestov, S. V., & Kuzin, S. V. 2016b, ApJ, 816, 90, doi: 10.3847/0004-637X/816/2/90

Savage, S. L., McKenzie, D. E., Reeves, K. K., Forbes, T. G., & Longcope, D. W. 2010, ApJ, 722, 329, doi: 10.1088/0004-637X/722/1/329

Scherrer, P. H., Bogart, R. S., Bush, R. I., et al. 1995, SoPh, 162, 129, doi: 10.1007/BF00733429

Seaton, D. B., Bartz, A. E., & Darnel, J. M. 2017, ApJ, 835, 139, doi: 10.3847/1538-4357/835/2/139

Seaton, D. B., & Darnel, J. M. 2018, ApJL, 852, L9, doi: 10.3847/2041-8213/aaa28e

Seaton, D. B., & Forbes, T. G. 2009, ApJ, 701, 348, doi: 10.1088/0004-637X/701/1/348

Somov, B. V. 2006, Plasma astrophysics, part II : reconnection and flares, Vol. 341, doi: 10.1007/978-0-387-68894-7

Sturrock, P. A. 1966, Nature, 211, 695, doi: 10.1038/211695a0

Sylwester, B., Faucher, P., Jakimiec, J., Krutov, V. V., & McWhirter, R. W. P. 1986, SoPh, 103, 67, doi: 10.1007/BF00154859

Urnov, A. M., Shestov, S. V., Bogachev, S. A., et al. 2007, Astron. Lett., 33, 396, doi: 10.1134/S1063773707060059

Veronig, A. M., Podladchikova, T., Dissauer, K., et al. 2018, ApJ, 868, 107, doi: 10.3847/1538-4357/aaeac5

Warren, H. P., Brooks, D. H., Ugarte-Urra, I., et al. 2018, ApJ, 854, 122, doi: 10.3847/1538-4357/aaa9b8

Webb, D. F., & Hundhausen, A. J. 1987, SoPh, 108, 383, doi: 10.1007/BF00214170

Wood, G. A. 1982, Exercise and Sport Sciences Reviews, 10, 308. http://journals.lww.com/acsm-essr/Abstract/1982/01000/DATA_SMOOTHING_AND_DIFFERENTIATION_PROCEDURES_IN.10.aspx

Yashiro, S., Gopalswamy, N., Michalek, G., et al. 2004, Journal of Geophysical Research (Space Physics), 109, 7105, doi: 10.1029/2003JA010282

Ye, J., Cai, Q., Shen, C., et al. 2020, ApJ, 897, 64, doi: 10.3847/1538-4357/ab93b5

Yokoyama, T., & Shibata, K. 1998, ApJL, 494, L113, doi: 10.1086/311174

Zhitnik, I. A., Bougaenko, O. I., Delaboudiniere, J.-P., et al. 2002, in ESA, Noordwijk, Vol. SP-506, Solar Variability: From Core to Outer Frontiers, ed. A. Wilson, 915–918

Zhitnik, I. A., Bugaenko, O. I., Ignat'ev, A. P., et al. 2003, MNRAS, 338, 67, doi: 10.1046/j.1365-8711.2003.06014.x

Zhu, C., Liu, R., Alexander, D., & McAteer, R. T. J. 2016,
    ApJL, 821, L29, doi: 10.3847/2041-8205/821/2/L29